Rotor-Flux Vector Based Observer of Interior Permanent Synchronous Machine

Marcin Morawiec ©, *Senior Member, IEEE*, Arkadiusz Lewicki ©, *Senior Member, IEEE*,
and Ikechukwu Charles Odeh ©, *Senior Member, IEEE*

***Abstract*—In this article, the sensorless control system of the interior permanent magnet synchronous motor (IPMSM) is considered. The control system is based on classical linear controllers. In IPMSM, there occurs nonsinusoidal distribution of rotor flux together with the slot harmonics, these are treated as control system disturbances. In this case, the classical observer structure in the (d-q) is unstable for the low range of rotor speed resulting in disturbances. This negative effect can be minimized by using the observer structure, which is based on the rotor flux vector in (α-β) stationary frame together with the classical rotor speed and position law of estimation. The performance of the observer structure is validated by simulation and experimental results in the sensorless control system with field-oriented control.**

***Index Terms*—Adaptive observer, sensorless control, speed observer.**

NOMENCLATURE

"^"	Estimated values.
"~"	Error of estimated values.
R_s	Stator resistance.
L_d, L_q	Winding inductances.
J, T_L, T_e	Inertia, load, and electromagnetic torque.
$i_{s\alpha, \beta}$	Stator current vector components.
$u_{s\alpha, \beta}$	Stator voltage vector components.
ψ_f	Permanent magnet flux linkage.
$\psi_{f\alpha, \beta}$	Permanent magnet flux components.
$\lambda_{\alpha, \beta}$	Rotor flux vector components.
ω_r	Rotor angular speed.
θ_r	Rotor position.

I. INTRODUCTION

THE interior permanent magnet synchronous motor (IPMSM) are used in many industrial systems, especially those with high drive requirements (precision of speed control and high dynamics of work). Most often, these machines are used in direct drives; that is, without mechanical gears. In this case, the low-speed motor is coupled directly to the working machine and the rotational speed is limited to several hundred rpm [1]. Slow-speed drives allow an increase in the efficiency of energy conversion due to the elimination of power losses in mechanical transmission. These drives are most often used in controlled machine tools, robotic drives, printing machines, benders, and traction vehicles [4]. Moreover, less system cost and improved robustness of the system are among the noticeable achievements of IPMSM sensorless control technology. The control technique of the IPMSM sensorless drive can be classified based on the speed of operation. For medium- and high-speed operation, the flux linkage model or back electromotive force model (EMF) can be used [2], [3]. There are two main IPMSM models which are based on the extended EMF (EEMF) and active flux concept. The characteristics of EEMF are mostly the same as the traditional EMF model. The only difference is that it shows an extra coupling in stator current dynamics and reluctance of IPMSM in the EEMF equation. The model based on active flux concept works on flux that generates torque needed to model the IPMSM. In this method, active flux can be determined by integrating the stator equivalent circuit. This approach faces parametric error and it is also influenced by the integration dc offset [2], [3], [4], [5]. In order to remove the nonlinearity of the mentioned models, a disturbance observer was proposed; which will first estimate the EEMF by disturbance observer, and then an adaptive observer will be used to extract the rotor position from EEMF [6], [7]. The synchronous reference frame model was implemented to estimate the rotor speed; however, it is concluded that this method is more sensitive to variation in the parameters [8], [9]. Model reference adaptive systems [10], sliding mode observers [11], [12], [25], extended state observers [13], [14], [15], [16], [17], [18], and adaptive filters [19], [20] are popular closed-loop observer techniques used for IPMSM drive (which are based on the EMF). To estimate rotor position and speed, a direct approach was proposed in [21] and [22]. In this approach, the inverse trigonometric function was used for estimating the position of the IPMSM rotor. This inverse trigonometric function was obtained from the estimated back EMF space vector. However, the estimated quality depends on back EMF; which might be distorted due to the nonlinearity of the inverter, parameter variation, and offset measurement. Deviation in the phase and

frequency can be experienced because of this distortion [23]. Moreover, it is noticed that IPMSM can be unobservable when the fundamental frequency observer gets to its limit at zero stator frequency and the back EMF reaches zero. Therefore, the methods based on the EEMF have weak properties for low-speed range of the rotor and should be applicable for the high-speed range.

In order to improve the properties of an observer system high-frequency (HF) voltage injection methods can be used [24], [25], [26], [27], [28], [29], [30], [31]. It has been shown in [26], [28], and [29] that HF voltage injection methods based on spatial variations in the inductance of motors can achieve satisfactory control performance; from zero speed to high speed under various loading conditions. In these methods, the injected HF voltages produce HF currents; from which the estimated error signal of the rotor position can be extracted. Another solution is to inject the sinusoidal current and estimate the position by using the virtual EMF [28], [29]. These methods, (HF injection of stator voltage) were recommended to a nonideal IPMSM machine; in which the spatial harmonics and/or nonsinusoidal distribution of EMF occurred [31]. However, sometimes the use of these methods is not straightforward in engineering practices due to the extensive sensorless control structure. For example, in [30], the sensorless control system was proposed in which the spatial harmonics are compensated by using repetitive control. The proposed method improves the estimation of rotor speed as well as rotor position; however, its industrial application is limited due to many tuning gains in the sensorless control scheme.

Herein, we propose rotor-flux, vector-based adaptive observer to estimate the speed and position values of IPMSM. In the presented IPM motor, both spatial harmonics and nonsinusoidal EMF occur. Due to the machine's asymmetry, the observer structure is based on the mathematical model in the α-β reference frame, in consideration of the rotor flux vector. However, the rotor speed and position are not calculated using the extended EMF mathematical model. The observer structure in the α-β reference frame is more robust in attending to disturbances because the state variables are not transformed through the estimated rotor position to the d-q reference frame. The rotor speed is estimated by using the conventional adaptive law ([3], [7], [8]); hence, the order of observer structure is decreased. The rotor position is determined by using the integration of the rotor speed value. In such a solution [3], [7], [8], the integrator is in the open loop and the observer structure can lose stability. Therefore, to improve the stability range and overall properties of the observer structure, we propose to introduce additional new feedback laws. Proposed stabilization functions are noncontinuous or constant; especially at low-speed range of the rotor or at standstill operation of the IPMSM. These additional injected functions to the adaptation law of the rotor speed and position satisfy the persistent excitation condition [27]. Also, they ensure the stability of the sensorless control system; especially for low-speed range with load torque injections. This approach is validated through theoretical, simulation, and experimental investigations in Sections III and IV.

The main contributions of this article are as follows.

- Development of an observer structure that is quite robust on disturbances (slot's harmonics, visible in Fig. 8). The observer structure is associated with the α-β reference frame, and it is assumed that the slot's harmonics are not compensated in the control system.
- Development of robust adaptive mechanism via additional stabilizing functions in the speed adaptation law.
- Improvement in the rotor position estimation due to the proposed robust stabilizing function; especially for low-speed range.

The proposed concept is verified through analytical and simulation results; validated by experimentation on IPMSM 3.5 kW machine with nonsinusoidal back-EMF distribution.

II. Mathematical Model of IPMSM

The mathematical model of IPMSM considered in this article is in the α-β reference frame [27], [31]

$$\frac{di_{s\alpha}}{d\tau} = \frac{\omega_r}{L_d}\lambda_\beta + (-R_s i_{s\alpha} + u_{s\alpha})L_1 + (-R_s i_{s\beta} + u_{s\beta})L_3 \tag{1}$$

$$\frac{di_{s\beta}}{d\tau} = -\frac{\omega_r}{L_d}\lambda_\alpha + (-R_s i_{s\alpha} + u_{s\alpha})L_3 + (-R_s i_{s\beta} + u_{s\beta})L_4 \tag{2}$$

$$\frac{d\omega_r}{d\tau} = \frac{1}{J}\left(\psi_{f\alpha}i_{s\beta} - \psi_{f\beta}i_{s\alpha} + (L_d - L_q)i_{s\alpha}i_{s\beta} - T_L\right) \tag{3}$$

$$\frac{d\theta_r}{d\tau} = \omega_r \tag{4}$$

where

$$\lambda_\alpha = L_d L_q^{-1}\psi_{f\alpha} - \left(1 - L_d L_q^{-1}\right)\left(L_0 i_{\alpha 2} + L_2 i_{s\alpha}\right) \tag{5}$$

$$\lambda_\beta = L_d L_q^{-1}\psi_{f\beta} + \left(1 - L_d L_q^{-1}\right)\left(L_0 i_{\beta 2} - L_2 i_{s\beta}\right) \tag{6}$$

where parameters L_0, L_2, and functions L_1, L_3, L_4, and the stator current Park transformation are defined in Appendix.

It is assumed that the machine parameters are known as unchanging in time. Operation domain D is defined as follows: $\boldsymbol{\lambda}^{\max}, \boldsymbol{i}_s^{\max}, \omega_r^{\max}$, and $T_L^{\max}$ mean the maximum values of rotor flux and stator current vectors, rotor speed, and load torque such that $|\boldsymbol{\lambda}| = \lambda^{\max}, |\boldsymbol{i}_s| \leq \boldsymbol{i}_s^{\max}, |\omega_r| \leq \omega_r^{\max}, T_L \leq T_L^{\max}$ where it is assumed $T_L^{\max} = T_{en}$ and $\boldsymbol{i}_s^{\max} \approx 1$ p.u.

The design of permanent magnet machines contains the sinusoidal and nonsinusoidal EMF distribution in which additional spatial harmonics can occur. In this article, the presence of nonsinusoidal EMF distribution in IPMSM is considered. The waveforms of nonsinusoidal EMF are presented in Fig. 8. The number of slots is 36 and the 18th harmonic is dominant. These harmonics are not compensated by using an extended control system like in [30]. In order to maintain the appropriate quality of the sensorless control, the occurrence of disturbances should be considered in the observer structure. Due to this, the design of the speed observer structures in many applications involves rigorous and complicated procedure. Herein, in the next section, the adaptive full-order observer is presented based on the model determined in (1) and (2) and the rotor flux dependencies (5) and (6) in the stationary α-β reference frame.

III. SPEED AND POSITION OBSERVER BASED ON ROTOR FLUX VECTOR

The adaptive mechanism for PMSM/IPMSM was presented in [2], [7], and [8]; therein, the analytical modeling was in (dq) reference frame. The use of the ideal model of IPMSM in this reference frame in the observer design procedure can lead to estimation errors and instability of the sensorless control. Hence, in this article, a solution is proffered which is based on the observer model in the stationary α-β reference frame connected to the stator. In this case, the speed observer structure is nonsymmetrical. This is because the proposed model contains the functions L_1, L_3, and L_4 introduced to (1) and (2); these functions are expressed in terms of the actual rotor position. Considering the mathematical model (1) and (2), the observer structure has the following form:

$$\frac{d\hat{i}_{s\alpha}}{d\tau} = \frac{\hat{\omega}_r}{L_d}\hat{\lambda}_\beta + \left(-R_s\hat{i}_{s\alpha} + u_{s\alpha}\right)L_1$$
$$+ \left(-R_s\hat{i}_{s\beta} + u_{s\beta}\right)L_3 + v_\alpha \tag{7}$$

$$\frac{d\hat{i}_{s\beta}}{d\tau} = -\frac{\hat{\omega}_r}{L_d}\hat{\lambda}_\alpha + \left(-R_s\hat{i}_{s\alpha} + u_{s\alpha}\right)L_3$$
$$+ \left(-R_s\hat{i}_{s\beta} + u_{s\beta}\right)L_4 + v_\beta \tag{8}$$

$$\frac{d\hat{\theta}_r}{d\tau} = \hat{\omega}_r + v_\theta \tag{9}$$

where $v_{\alpha,\beta}$, and v_θ are stabilizing functions in (7) and (8); and their form will be determined by using the stability of the Lyapunov method, and $u_{s\alpha,\beta}$ are treated as known values.

The rotor flux vector components can be estimated using (5) and (6) as follows:

$$\hat{\lambda}_\alpha = L_d L_q^{-1}\psi_{f\alpha} - \left(1 - L_d L_q^{-1}\right)\left(L_0\hat{i}_{\alpha 2} + L_2\hat{i}_{s\alpha}\right) \tag{10}$$

$$\hat{\lambda}_\beta = L_d L_q^{-1}\psi_{f\beta} + \left(1 - L_d L_q^{-1}\right)\left(L_0\hat{i}_{\beta 2} - L_2\hat{i}_{s\beta}\right). \tag{11}$$

Remark 1: It is assumed that in the observer structure (7)–(11), the functions L_1, L_3, L_4, and $i_{\alpha 2}$, $i_{\beta 2}$, $\psi_{f\alpha,\beta}$ the estimated value of rotor position and stator current vector components $\hat{i}_{s\alpha,\beta}$ are used, which were defined as follows:

$$L_1 = L_d^{-1}\cos^2\hat{\theta}_r + L_q^{-1}\sin^2\hat{\theta}_r, \ L_3 = 0.5\left(L_d^{-1} - L_q^{-1}\right)\sin(2\hat{\theta}_r) \tag{12}$$

$$L_4 = L_d^{-1}\sin^2\hat{\theta}_r + L_q^{-1}\cos^2\hat{\theta}_r, \ \hat{i}_{\alpha 2} = \hat{i}_{s\alpha}\cos 2\hat{\theta}_r + \hat{i}_{s\beta}\sin 2\hat{\theta}_r \tag{13}$$

$$\hat{i}_{\beta 2} = -\hat{i}_{s\alpha}\sin 2\hat{\theta}_r + \hat{i}_{s\beta}\cos 2\hat{\theta}_r \tag{14}$$

and L_0, L_2 are defined in Appendix.

The designing procedure requires two steps. In the first step, stability analysis should be provided to stabilize the observer structure. The introduced stabilizing functions (7)–(9) stabilizing function has to satisfy the Lyapunov stability theorem in which the chosen candidate function V should be positively determined. The quadratic Lyapunov function has the following form:

$$V = 0.5\left(\left(\tilde{i}_{s\alpha}^2 + \tilde{i}_{s\beta}^2\right) + \tilde{\theta}_r^2\right) \tag{15}$$

where the following deviations are assumed:

$$\tilde{i}_{s\alpha,\beta} = \hat{i}_{s\alpha,\beta} - i_{s\alpha,\beta}, \ \tilde{\omega}_r = \hat{\omega}_r - \omega_r, \ \tilde{\theta}_r = \hat{\theta}_r - \theta_r. \tag{16}$$

The derivative of the Lyapunov function should be negatively determined; that is $\dot{V} \leq 0$. Appropriate substitutions in the derivative of (15) yields

$$\dot{V} = \tilde{i}_\alpha \Bigg(L_d^{-1}(\hat{\omega}_r(\hat{\lambda}_\beta - \tilde{\lambda}_\beta) - \tilde{\omega}_r(\hat{\lambda}_\beta - \tilde{\lambda}_\beta)$$
$$- R_s(\tilde{i}_{s\alpha}L_1 + \tilde{i}_{s\beta}L_3) + v_\alpha\Bigg)$$
$$+ \tilde{i}_\beta\Bigg(-L_d^{-1}(\hat{\omega}_r(\hat{\lambda}_\alpha - \tilde{\lambda}_\alpha) - \tilde{\omega}_r(\hat{\lambda}_\alpha - \tilde{\lambda}_\alpha)$$
$$- R_s(\tilde{i}_{s\alpha}L_3 + \tilde{i}_{s\beta}L_4) + v_\beta\Bigg)$$
$$+ \tilde{\theta}_r\left(\tilde{\omega}_r + v_\theta\right) \leq 0. \tag{17}$$

The observer structure is asymptotic stable if the stabilizing functions have the form

$$v_\alpha = -c_\alpha R_s L_1 \tilde{i}_{s\alpha} + c_\lambda L_d^{-1}\hat{\omega}_r\hat{\lambda}_\beta\tilde{i}_{s\alpha} \tag{18}$$

$$v_\beta = -c_\alpha R_s L_4 \tilde{i}_{s\beta} - c_\lambda L_d^{-1}\hat{\omega}_r\hat{\lambda}_\alpha\tilde{i}_{s\beta} \tag{19}$$

$$v_\theta = -c_\theta\tilde{\theta}_r \tag{20}$$

where c_α, c_θ, $c_\lambda > 0$ are introduced to the stabilizing functions in (7)–(9) tuning gains of the observer.

In order to estimate the rotor speed, the Lyapunov function in (15) should be extended to the rotor speed deviation term $V_1 = \gamma^{-1}\tilde{\omega}_r^2$. Thus, the derivative of the Lyapunov function assumes the form

$$\dot{V} = \tilde{\omega}_r L_d^{-1}\left(-\hat{\lambda}_\beta\tilde{i}_{s\alpha} + \hat{\lambda}_\alpha\tilde{i}_{s\beta} + \frac{1}{\gamma}\dot{\omega}_r\right) \leq 0. \tag{21}$$

The rotor speed value can be estimated by using the adaptation mechanism directly from (21)

$$\dot{\hat{\omega}}_r = \gamma L_d^{-1}(\hat{\lambda}_\beta\tilde{i}_{s\alpha} - \hat{\lambda}_\alpha\tilde{i}_{s\beta}) \text{ for } \gamma > 0 \text{ and } \dot{\hat{\omega}}_r \approx \dot{\omega}_r. \tag{22}$$

Further considerations will demonstrate that the estimation errors can exponentially converge to zero in finite time $t > t_1$. Then, since the system (1) and (2) stays in operation domain D, hence if

$$c_{\alpha 1} = \max\left\{\tilde{i}_{s\alpha}R_s L_1\right\} + \delta_1 \tag{23}$$

$$c_{\alpha 2} = \max\left\{\tilde{i}_{s\beta}R_s L_4\right\} + \delta_2 \tag{24}$$

$$c_\theta = \max\left\{\tilde{\theta}_r\omega_r^{-1}\right\} + \delta_\theta \tag{25}$$

with δ_1, δ_2, $\delta_\theta > 0$ and for $\tilde{i}_{s\alpha,\beta} \leq \varepsilon_1$, $\tilde{\theta}_r \leq \varepsilon_2$, $\tilde{\omega}_r \leq \varepsilon_3$ and $\varepsilon_{1,2,3} << 1$ are sufficient small reals, the derivative of the Lyapunov function takes the following form:

$$\dot{V} = -\delta_\alpha\left|\tilde{i}_{s\alpha}\right| - \delta_\beta\left|\tilde{i}_{s\beta}\right| - \delta_\theta\left|\tilde{\theta}_r\right| \leq -\mu\sqrt{V} \tag{26}$$

Fig. 1. Space vector representation of IPMSM in the α-β plane.

where $\mu = \min(\sqrt{2}\delta_\alpha, \sqrt{2}\delta_\beta, \sqrt{2}\delta_\theta)$ and $\delta_\alpha = \delta_1 + \delta_2$.

The condition (26) implies the convergence of vector values $\hat{\boldsymbol{i}}_s$ to $\boldsymbol{i}_s$ and $\hat{\vec{\lambda}}$ to $\boldsymbol{\lambda}$. Hence, $\hat{\theta}_r$ tend to real value θ_r in finite time, denoted as t_2. For $(\hat{\lambda}_\beta \tilde{i}_{s\alpha} - \hat{\lambda}_\alpha \tilde{i}_{s\beta}) \neq 0$ and $\gamma \geq 0$ the rotor angular speed estimated from (22) converges exponentially to its real value ω_r. Assuming that $c_\alpha = c_{\alpha 1} = c_{\alpha 2}$, the value of c_α can be determined as follows:

$$c_\alpha = \max\left\{ R_s \tilde{i}_{s\alpha} \sqrt{L_1^2 + L_4^2} \right\} \tag{27}$$

and value of c_λ can be determined (assuming $c_\alpha = 1$ and $|\hat{\omega}_r|(\hat{\lambda}_\alpha^2 + \hat{\lambda}_\beta^2) \neq 0$) in the following form:

$$0 \leq c_\lambda \leq \frac{R_s L_1 \hat{\lambda}_\beta - R_s L_4 \hat{\lambda}_\alpha}{L_d^{-1} |\hat{\omega}_r| (\hat{\lambda}_\alpha^2 + \hat{\lambda}_\beta^2)}. \tag{28}$$

Remark 2: In (20), there exists the estimation error of the rotor position. The rotor position error is not available, because in the sensorless control system, the rotor position and speed are not measured. Therefore, the deviation $\tilde{\theta}_r$ can be replaced with the approximated value of this deviation and then (20) is rewritten

$$v_\theta = -c_\theta \tilde{\theta}_\lambda. \tag{29}$$

The vectors in the machine rotate with the synchronous angular speed of the flux vector of the permanent magnets ω_f; whose value is equal to the rotor angular speed. The rotor position is equal to the position of the flux vector of permanent magnets. Therefore, the deviation between two positions of the rotor flux vectors in which one of them is estimated from (10) and (11) and the second is calculated from (5) and (6) can be calculated from

$$\tilde{\theta}_\lambda = \tan^{-1}(\varphi) \tag{30}$$

where $\varphi = (\lambda_\alpha \hat{\lambda}_\beta - \lambda_\beta \hat{\lambda}_\alpha)(\lambda_\alpha \hat{\lambda}_\alpha + \lambda_\beta \hat{\lambda}_\beta)^{-1}$ and the rotor flux vector components $\lambda_{\alpha,\beta}$ can be determined from (5) and (6) in which it is assumed $\theta_r \approx \hat{\theta}_r$ and the measured values of $i_{s\alpha,\beta}$ are used and $(\lambda_\alpha \hat{\lambda}_\alpha + \lambda_\beta \hat{\lambda}_\beta) \neq 0$. Value $\tilde{\theta}_\lambda$ can be projected using

$$\tilde{\theta}_\lambda = \begin{cases} \tilde{\theta}_\lambda - \pi/2, \varphi \geq 0 \\ \tilde{\theta}_\lambda + \pi/2, \varphi < 0 \end{cases}. \tag{31}$$

The value $\tilde{\theta}_\lambda$ is close to zero and after amplifying, this value can be $\tilde{\theta}_r \approx \tilde{\theta}_\lambda$. The angle defined in (30) was shown in Fig. 1.

Remark 3: The rotor speed value in the proposed observer structure is estimated from (22). The estimated value of the rotor speed is dependent on the stator current error and rotor flux vector components. In (22), there is a cross product of these

vectors. It can be noticed that for different working points of the IPMSM, the mutual position of these vectors does not have the same value. For the ideal case, if these vectors are perpendicular, their scalar product is equal to zero. In practice, the scalar product of these two vectors is close to zero but not zero for the observer gains (27) and (28). It implies that the estimated rotor speed error will be proportional to the scalar product of these two vectors (which will be proved by using the simulation results). Therefore, to improve the robustness of the speed observer, it is proposed in this article to introduce the updated estimation law, which is based on the cross and scalar product of the rotor flux and stator current errors. The estimation law (22) can be modified to the following form:

$$\dot{\hat{\omega}}_r = \gamma L_d^{-1}\left(\hat{\lambda}_\beta \tilde{i}_{s\alpha} - \hat{\lambda}_\alpha \tilde{i}_{s\beta} - k_c s_\omega \right) \tag{32}$$

where

$$s_\omega = \left(\hat{\lambda}_\alpha \tilde{i}_{s\alpha} + \hat{\lambda}_\beta \tilde{i}_{s\beta} \right) \tag{33}$$

and $|s_\omega| \leq \varepsilon_\omega$ its value to be bounded.

Gain k_c has an important meaning when the machine is passing through zero speed. From the observability condition, the position and speed observer system are observable for the rotor speed $\omega_r \neq 0$ or the four conditions are satisfied [27]. For the zero speed range, the additional observer couplings (9), (32) cause the value of s_ω is always different from zero; and has a higher value than in the different working points. This is particularly visible in simulation and experimental results. It means that the rotor angular speed is estimated with low accuracy, which influences the rotor position estimation. The rotor position directly depends on the estimated rotor speed value. Deterioration of the estimation process is caused by the mutual position of the rotor flux and estimated stator current error vectors. This is the cross product and its value influences the scalar product which is in the term s_ω. Therefore, the value of s_ω after amplification is converged to rotor speed estimation error (phase of its oscillation as well as values), hence through the implication the transient (value and phase) of the stabilizing function (29) is close to position estimation error.

The tuning gains can be specified from the model of the observer errors linearized near an equilibrium point in the d-q reference frame. This model is connected to the flux ψ_f, which is based on the mathematical model in (dq) reference frame [2], [4], [5], [6], [7], [8]. The general form of the linearized system is

$$\frac{d}{dt}\Delta\mathbf{x}(t) = \mathbf{A}\Delta\mathbf{x}(t) + \mathbf{B}\Delta\mathbf{u}(t) \tag{34}$$

where $\mathbf{A}$, $\mathbf{B}$ are the Jacobian matrices and $\Delta\mathbf{x}(t) = [\tilde{i}_{sd}, \tilde{i}_{sq}, \tilde{\omega}_r, \tilde{\theta}_r]^T$, $\Delta\mathbf{u}(t)$ is treated as known control inputs.

By using the observer errors (16) for (dq), the matrix $\mathbf{A}$ of the observer system can be determined as follows:

$$\mathbf{A} = \begin{bmatrix} -a_1(1+c_\alpha) & a_2\omega_r^*(1+c_\lambda) & a_2 i_{sq}^* & 0 \\ -a_3\omega_r^*(1+c_\lambda) & -a_4(1+c_\alpha) & -a_3 i_{sd}^* & 0 \\ -\gamma a_2(i_{sq}^* - k_c i_{sq}^*) & \gamma a_3(i_{sd}^* + k_c i_{sq}^*) & 0 & 0 \\ 0 & 0 & 1 & -c_\theta \end{bmatrix} \tag{35}$$
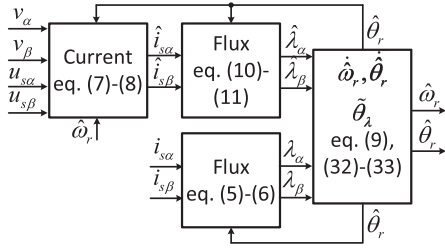
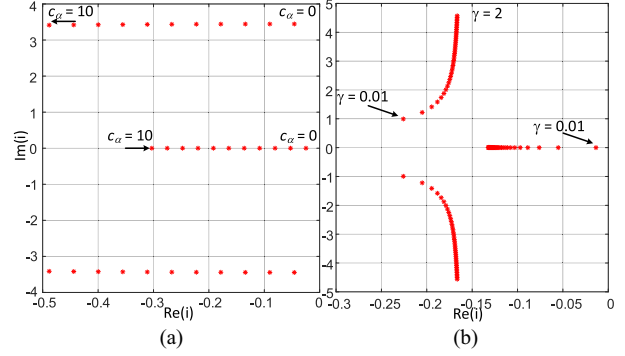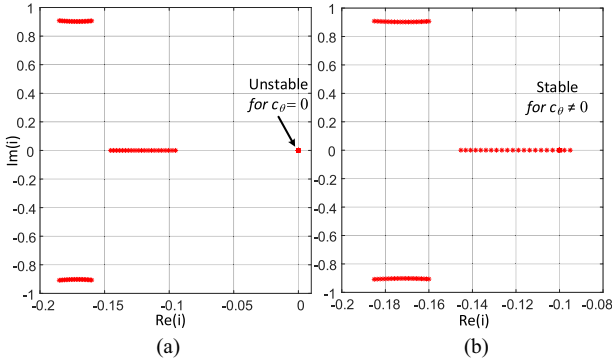Fig. 2. Simplified speed and position observer structure scheme.

Fig. 3. Spectrum of matrix **A** of the linearized observer system for $c_\alpha = 3.0$, $c_\lambda = 0.05$, $k_c = 0.5$, $T_L = 1$, $\omega_r = 0$ p.u. and (a) $c_\theta = 0$, (b) $c_\theta = 0.1$ p.u.
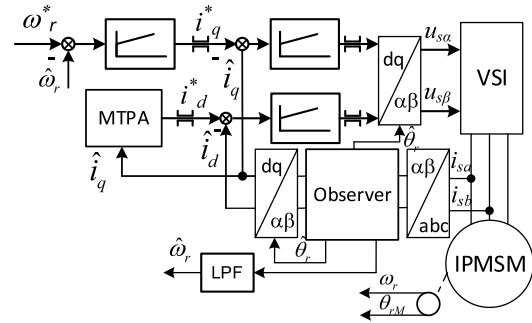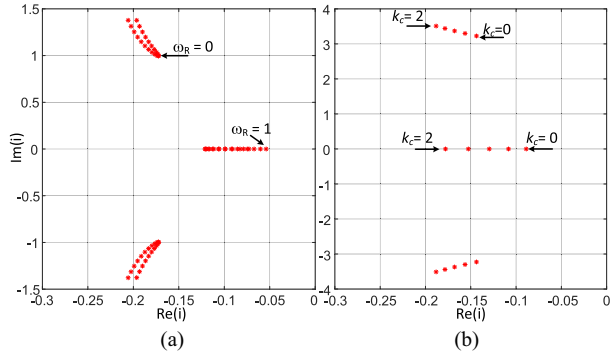

Fig. 4. Spectrum of matrix **A** of the linearized observer system for $c_\alpha = 3.0$, $c_\lambda = 0.05$, $T_L = 1$, $c_\theta = 1$ and for: (a) rotor speed is changing from −1.0 to 1.0 p.u. and $k_c = 0.5$, (b) k_c is changing from 0 to 2.0 p.u. and $\omega_r = 1.0$ p.u.

where $a_1 = R_s L_d^{-1}$, $a_2 = L_q L_d^{-1}$, $a_3 = L_d L_q^{-1}$, $a_4 = R_s L_q^{-1}$, and $i^*_{sd,\ q}$ imply the values determined from the working point. This point can be obtained from $i^*_{sq} = T_L/(\psi_f + (L_d - L_q)i^*_{sd})$. It is assumed that $i^*_{sd} = -0.05$ p.u., $\omega^*_r = \omega_r$.

In Fig. 3(a), the rotor speed is $\omega_r = 0$ p.u. and the load torque is equal to 1.0 p.u. For $c_\theta = 0$, the observer structure is unstable due to the open integrator form of (9) – one pole of the system is always equal to zero. For $c_\theta \neq 0$, the system is stable [Fig. 3(b)]. In Fig. 4(a), the rotor speed is changed from −1.0 to 1.0 p.u. and the load torque is equal to 1.0 p.u. In Fig. 4(b), gain k_c in (32) is changed from 0 up to 2.0 p.u.

For $k_c = 0$, the observer pole is close to the zero point but for $k_c = 2$, it drifts away from zero. However, oscillations can occur due to the imaginary value of the poles. The same phenomenon

Fig. 5. Spectrum of matrix **A** of the linearized observer system for $c_\lambda = 0.05$, $k_c = 0.5$, $T_L = 1$, $\omega_r = 1.0$ p.u., $c_\theta = 1$ and for: (a) c_α is changing from 0 to 10 p.u. and (b) γ is changing from 0.01 to 2.0 p.u. and $c_\alpha = 3.0$ p.u.

Fig. 6. Sensorless control scheme of the IPMSM machine.

goes for c_α gains; this is visible in Fig. 5(a). In Fig. 5(b), γ is changed from 0.01 up to 2. For $\gamma = 0.01$ one of the poles is close to zero. For $\gamma = 2$, the system is more stable because the poles are at some distance away from the zero point; but oscillations are increased. In summary, the presented stability analyses in this section confirm that the value of the observer tuning gains is close to the approximation values from (27) and (28). For $c_\theta = 0$, the observer structure is unstable and in order to improve the stability range the observer gains should be: $c_\alpha \gg 1.0$ and $k_c > 0$. Properties of the proposed solution allow replacing in (20) estimated position error value $\tilde{\theta}_r \equiv \tilde{\theta}_\lambda$ and rewriting (32) in the form $\dot{\hat{\omega}}_r = \gamma L_d^{-1}(\hat{\lambda}_\beta \tilde{i}_{s\alpha} - \hat{\lambda}_\alpha \tilde{i}_{s\beta} - \tilde{\omega}_r)$. It then follows that the assumption (22), where $\dot{\tilde{\omega}}_r \approx \dot{\hat{\omega}}_r$ and $\dot{\omega}_r = 0$, is correct and justified.

The speed and position observer structure scheme is presented in Fig. 2. In the sensorless control system scheme shown in Fig. 6, the classical FOC is implemented by using the MTPA algorithm [2], [27] or field weakening method [31]. In this control system, the phase stator currents (a, b) are measured and transformed to α-β reference frame. In order to obtain the currents in d-q frame, Park's transformation was used [31]. The observer gains in the simulation and experiment were: $c_\alpha = 3.0$, $c_\lambda = 0.001$, $k_c = 0.1$, $c_\theta = 0.15$ in p.u.

In Fig. 7, chosen simulation results are presented. In order to confirm the theoretical hypothesis, the IPMSM is starting up to 2.0 p.u. [Fig. 7(a)]. The estimated $\hat{i}_{sq}$, s_ω defined in (33), estimated rotor position $\hat{\theta}_r$ and $\tilde{\theta}_\lambda$ defined in (31) are shown.
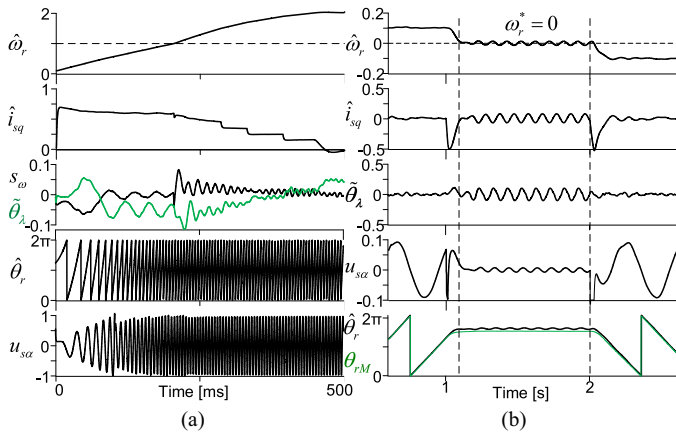
Fig. 7. Simulation results for (a) machine is starting-up to 2.0 p.u., (b) standstill machine test, machine is not-loaded ($T_L = 0.02$ p.u.).

TABLE I
IPMSM PARAMETERS AND REFERENCES UNIT

Symbol	Quantity	Values
R_{sN}	Stator resistance	0.035 p.u.
L_{dN}	d-axis inductance	0.28 p.u.
L_{qN}	q-axis inductance	0.82 p.u.
ψ_f	Permanent magnets flux linkage	0.89 p.u.
T_{eN}	Nominal value of electromagnetic torque	0.81 p.u.
P_n	Nominal power	3.5 kW
I_n	Nominal stator current (Y)	7.5 A
U_n	Nominal stator voltage (Y)	285 V
n	Nominal rotor speed	1500 rpm
f	Nominal frequency	50 Hz
$U_b = U_n$	Reference voltage	285 V
$I_b = I_n\sqrt{3}$	Reference current	12.97 A

Fig. 8. Stationary state of the machine. Measured (a) phase "A" EMF voltage, (b) phase to phase "A-B" EMF voltage.
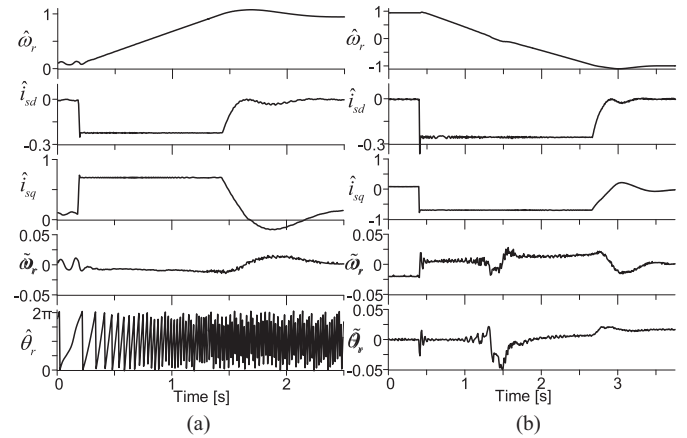
Fig. 9. IPMSM (a) is starting up from 0.1 to 1.0 p.u. for (a) sensorless control system with the proposed observer, (b) is reversing up to −1.0 p.u.

The machine is field-weakened [31]. In Fig. 7(b), after 1 s the reference speed is changed from 0.1 to 0 p.u. and after 2 s to −0.2 p.u. The same variables are displayed as in Fig. 7(a), together with the measured rotor position θ_{rM}. The IPMSM is not loaded ($T_L = 0.02$ p.u.). During standstill, there is a visible, how the proposed stabilizing function $\tilde{\theta}_\lambda$ prevents the sensorless control system from being unstable in the unstable range. The proposed function, $\tilde{\theta}_\lambda$, has a value smaller than 0.1 p.u. (it depends on the load torque T_L) and it is not constant but almost sinusoidal. This value influences the voltage vector components, $u_{s\alpha,\beta}$ [Fig. 7(b) $u_{s\alpha}$ waveform], and averts loss of stability ($u_{s\alpha,\beta} = 0$), (condition of stability are given in [27]).

As shown in Fig. 7 the simulation results confirm that the sensorless control system is stable for rotor speed higher than the nominal; as well as for the standstill operation.

In the next sections, the chosen experimental results will confirm the above theoretical hypothesis.

IV. EXPERIMENTAL RESULTS

The experimental tests were carried out on a 3.5 kW drive system with the nonsinusoidal back-EFM distribution, supplied by the VSC. The electric drive system parameters are given in Table I. The control system was implemented in an interface with a *DSP Sharc* ADSP21363 floating-point signal processor

and Altera Cyclone 2 FPGA. The sampling time was 150 µs (6.6 kHz) and the transistor switching frequency was 3.3 kHz. In the DSP board, the control system structure from Fig. 6 was presented. The control system computational time is about 49 µs (is increasing due to trigonometric function calculation) without code optimization.

In Fig. 8(a), the experimental measured phase "A" EMF voltage of the IPMSM is shown. This waveform confirms the nonsinusoidal EMF distribution in the machine. In Fig. 8(b), the measured "A-B" EMF voltage of IPMSM is shown. In both waveforms, the slot harmonics are visible. The speed observer is based on the sinusoidal machine model. Therefore, the additional slots harmonics and nonsinusoidal shape are treated as the observer system disturbances, which have bounded value and frequency.

These disturbances have great importance during the low speed of IPMSM operation under sensorless control conditions. This is visible close to 0.1 p.u. rotor speed without the load torque Figs. 9(a) and 10(b).

In order to show the properties of the proposed observer the experimental verifications have been divided into four scenarios:

1st – machine start-up and speed reversal;
2nd – standstill and load torque injections for medium speed;
3rd – low-speed operation under load torque;
4th – nominal parameters uncertainties.

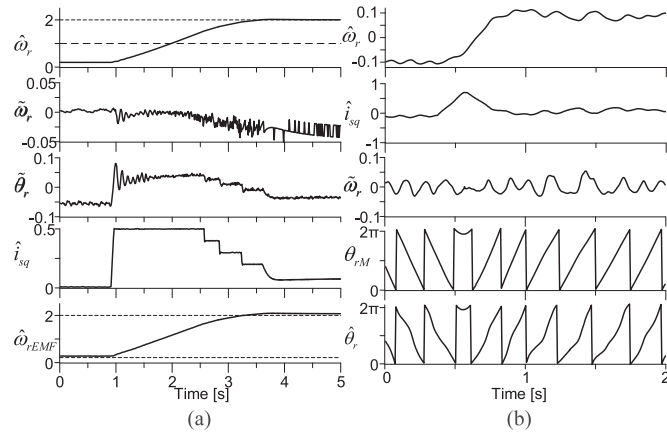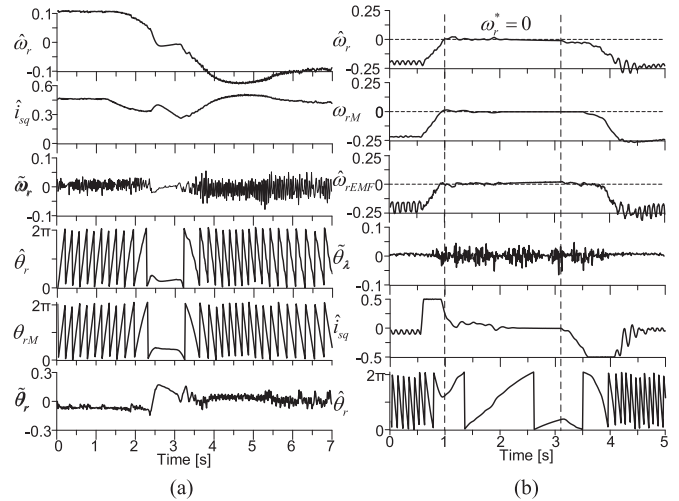Fig. 10. IPMSM is not loaded and (a) starting up to 2.0 p.u., (b) reversing from −0.1 to 0.1 p.u.

Fig. 11. (a) Rotor speed is changed from 0.1 to −0.1 p.u., $T_L = 0.5$ p.u. (b) Machine standstill test is shown without load $T_L = 0.05$ p.u.

In the experimental results, the estimated stator current components $\hat{i}_{sd}$, $\hat{i}_{sq}$, rotor speed $\hat{\omega}_r$, and rotor position $\hat{\theta}_r$ as well as measured rotor position θ_{rM}. The nominal value of electromagnetic torque is $T_{en} \approx 0.8$ p.u. (for the nominal value of stator current), however, in Fig. 14(b) this value is increased up to 150% ($T_L^{\max} = 1.5T_{en} \approx 1.3$) to show the behavior of the sensorless control system.

A. Drive Starting and Reversal

The first scenario is presented in Figs. 9 and 10. In Fig. 9, the machine is starting up from 0.1 to 1.0 p.u., and the load torque was about 0.1 p.u. during this test. In Fig. 9(a), the waveforms of indicated variables are shown in the sensorless control system. The estimated rotor speed error is smaller than 0.02 p.u. in the dynamic states. In Fig. 9(b), the machine is reversing from 1.0 to −1.0 p.u. The rotor speed error during the zero-crossing is smaller than 0.025 p.u; also the estimated position error is smaller than 0.05 p.u.

In Fig. 10(a), test result for high value of rotor speed is shown. The machine is field-weakened, similarly as shown in Section III – [Fig. 7(a)]; and the value of the rotor speed is two times the nominal. The rotor position error is smaller than 0.05 p.u. in the dynamic state and the average rotor speed error is ~0.025 p.u. for the rotor speed value of 2.0 p.u.

In addition to the presented variables, the speed value $\hat{\omega}_{rEMF}$ is estimated by using the back-EMF observer [8] is also shown, for comparison. As seen, the value of $\hat{\omega}_{rEMF}$ estimated with 0.07 p.u. error for the low speed, and about 0.12 p.u. for the high speed (2.0 p.u.).

In Fig. 10(b), the IPMSM is reversing from −0.1 to 0.1 p.u. on no-load at the estimated rotor speed. The oscillation value depends on the reluctance torque as well as on the slot's harmonics and trapezoidal EMF distribution which are visible in Fig. 8. These are treated as disturbances to the observer system. For this case, the higher oscillations cannot be damped in the observer structure by using other sets of gains. This effect occurs when the machine is on no-load. The oscillations can be compensated if the control system from Fig. 6 will be extended to the damping

structure presented, e.g., in [30]. However, this article focuses only on the speed observer structure and the nonsinusoidal EMF is treated as the observer's disturbances. To minimize this effect the LPF of the estimated rotor speed is introduced.

In Fig. 11(a), the rotor speed reverse under load torque, $T_L = 0.5$ p.u. The rotor speed error is less than 0.05 p.u. and the error of the rotor speed position is about 0.2 p.u. during the zero-value of rotor speed (the ramp-time is set to about 2 s).

In Fig. 11(b), the rotor speed is changed from −0.2 to 0 p.u. (for 2 s) and again to −0.2 p.u., after 3 s. The load torque value is about 0.05 p.u. The average value of the rotor speed error is less than 0.02 p.u. The rotor is at a standstill [the same condition as in Fig. 7(b)]; however, the estimated value of the rotor position, $\hat{\theta}_r$, changed. This behavior results from the estimation law (9) in which the rotor position is determined from the integration of the estimated rotor speed as well as from the stabilization law $v_\theta = -c_\theta \tilde{\theta}_\lambda$. The values of the function $\tilde{\theta}_\lambda$ are shown in Fig. 11(b). It prevents the IPMSM machine from getting stuck and losing synchronization.

B. Load Torque Injections

In the second scenario, the rotor speed was set to 0.5 p.u. and after 0.2 s load torque was increased to $T_L = 0.85$ p.u. For this test, the stator current i_{sq} value is limited in the control system to 1.0 p.u., as shown in Fig. 12(a). Therein, the estimated rotor speed $\hat{\omega}_r$, stator current components $\hat{i}_{sd}$, $\hat{i}_{sq}$, estimated and measured values of rotor position $\hat{\theta}_r$, θ_{rM} are also displayed. In Fig. 12(b), the same machine working points are presented but in a small-time period of 150 ms. It is obvious that the estimated rotor speed error in the steady-state is about 0.01 p.u.; and the estimated and measured rotor position are converged to each other. The calculated average value of the rotor position error for this case is less than 0.015 p.u.
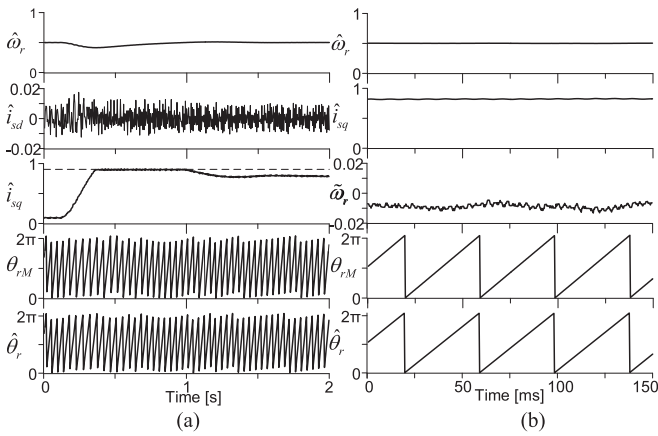
Fig. 12. Machine is loaded (a) after 0.2 s the load torque $T_L \sim$ 0.85 p.u. is added, (b) stationary state is presented in 150 ms period.
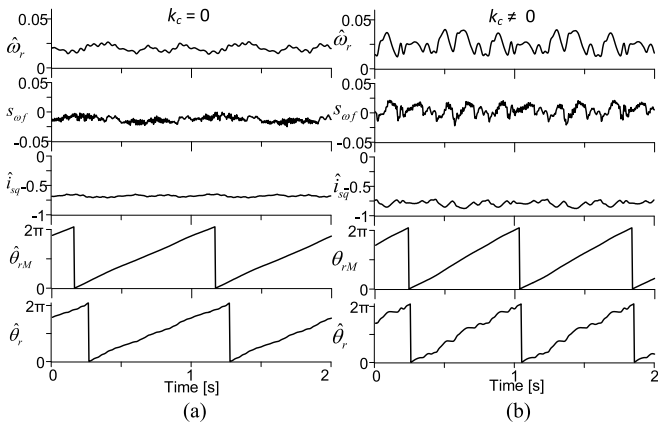

Fig. 13. Regenerating mode of IPMSM machine for the low reference speed 0.025 p.u., $T_L = -0.75$ p.u. for the cases (a) in (32) $k_c = 0$, (b) in (32) $k_c = 1.5$ p.u.
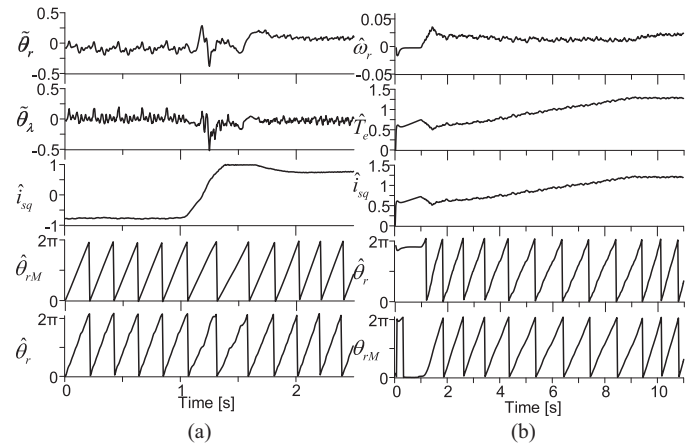

Fig. 14. (a) Load torque is changed from regenerating T_L −0.85 to motoring mode 0.85 p.u. The rotor speed was 0.2 p.u. (b) rotor speed is set to 0.02 p.u., and the machine is loaded $T_L = 1.25$ p.u. ($1.5T_{eN}$).
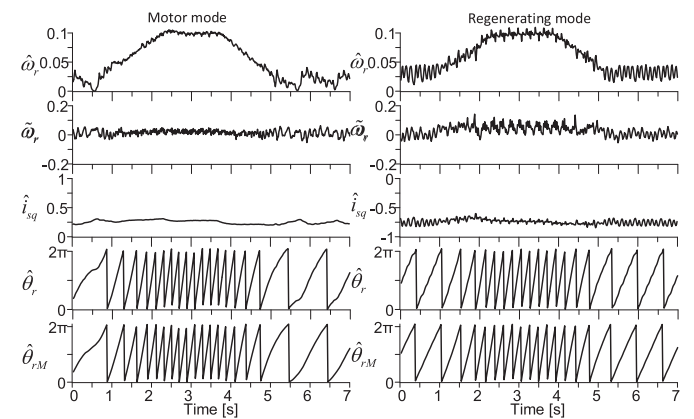
Fig. 15. Rotor speed is changed from 0.025 to 0.1 p.u. for (a) load torque is $T_L = 0.75$, (b) load torque is $T_L = -0.75$ p.u.

C. Low Speed and the Regenerating Mode

In this scenario, the behavior of the observer system was checked during the changes in load torque values of IPMSM (from motoring mode to regenerating mode). In Fig. 13, the regenerating mode of the machine is presented. The rotor speed is set to 0.025 p.u. for two cases: the observer gain is set to $k_c = 0$. For $k_c = 0$, the load torque is about −0.75 p.u. and the rotor position error is about 0.15–0.2%. The sensorless control structure is stable, however, the properties of the observer structure are poor. The estimated stator current component $\hat{i}_{sq}$ value should be equal to −0.75 p.u. but, its value is about −0.65 p.u. in Fig. 13(a); due to the rotor position error. It means that in the low-speed range and the regenerating machine mode, value of the variable s_ω has an average value different than zero. The vectors of the estimated rotor flux from (10) and (11) and the vector of stator current error are not perpendicular. Hence, the value of the scalar product s_ω is constant and below the zero. In Fig. 13(a), $s_{\omega f}$ is filtrated value of s_ω when low-pass filter (with the time constant equal to $1/T_i = 0.05$ p.u.) is used. The same waveforms but for $k_c = 1.5$ p.u. are presented in Fig. 13(b). In this case, the rotor position error is less than 2%–3%; the average

value of $s_{\omega f}$ is almost zero; and the stator current $\hat{i}_{sq}$ value is −0.75 p.u. It implies that the sensorless control system with $k_c \neq 0$ is more robust on disturbances than with $k_c = 0$. In the former case, they are the nonsinusoidal EMF and the slots harmonics from Fig. 8. This is the main contribution of this article. The oscillations are visible in Fig. 13(b) resulting from the gained value of $k_c s_\omega$ in (32).

In Fig. 14(a), the motor and regenerating modes of the machine are presented. The rotor speed was 0.2 p.u. and after 1 s the load torque command is changed from −0.85 to 0.85 p.u. (on the ramp about 0.5 s). The instantaneous rotor position error was about 0.2 p.u. when the electromagnetic torque was close to zero and changing its value from negative to positive. The value of the deviation $\tilde{\theta}_\lambda$ in (29) is converged to $\tilde{\theta}_r$. This is visible in Fig. 14(a) and confirms the assumption in Remark 2. In Fig. 14(b), the rotor speed is set to 0.02 p.u. and the load torque is 1.25 p.u. ($T_L = 1.5T_{eN}$). The error of estimated rotor speed is smaller than 0.01 p.u. error of rotor position is smaller than 0.03 p.u. in the steady-state.

In Fig. 15(a), the motoring mode of IPMSM is presented. The $T_L = 0.75$ p.u. and the rotor speed is changed from 0.025 to
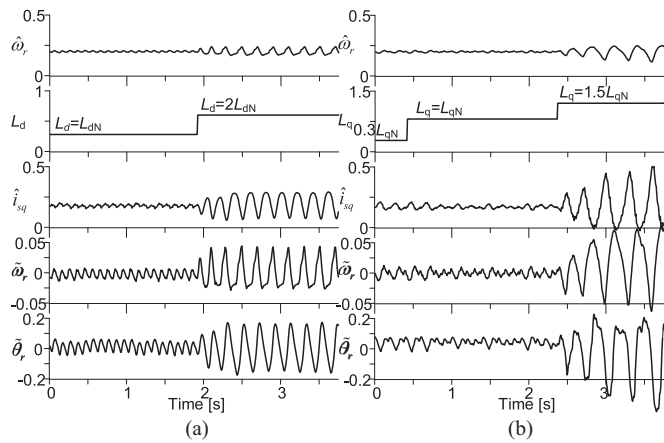
Fig. 16. Machine is loaded at about 0.35 p.u. value of load torque, the rotor speed is 0.2 p.u. for different value of inductances. (a) L_d. (b) L_q.

0.1 p.u. The rotor speed has oscillation visible in the estimated rotor speed transients during the very low speed of 0.025 p.u. In Fig. 15(b), the regenerating mode of IPMSM is shown. $T_L = -0.75$ p.u. and the rotor speed is changing from 0.025 to 0.1 p.u. (by using the ramp time ~ 2 s for both cases).

D. Uncertainty of Machine Parameters

In Fig. 16, the test of robustness on the changes of the nominal inductances $L_{d,q}$ of IPMSM is presented. The reference rotor speed is 0.2 p.u. and machine is loaded $T_L = 0.3$ p.u. In the sensorless control system after 2 s, the inductance $L_d = 2L_{dN}$ [Fig. 16(a)]. The estimated rotor speed and position errors were 0.05 and 0.2 p.u. properly. In Fig. 16(b), in 0 s, the value of the L_q $= 0.3L_{qN}$ and after 0.5 s $L_q = L_{qN}$ and after 2.5 s $L_q = 1.5L_{qN}$. For $L_q = 1.5L_{qN}$, the observer is on the verge of stability. The error of estimated rotor position is higher than 0.35 p.u.

The sensorless control system is robust on the changes of the inductance L_d up to $2L_{dN}$ without losing of stability; however, for the inductance L_q the maximum change is $1.5L_{qN}$. Higher value leads to loss of stability, which is visible in Fig. 16(b).

V. DISCUSSION

The presented experimental results of sensorless FOC control of IPMSM validate the good properties of the proposed adaptive speed and position observer for 0.02 p.u. (30 rpm); with injected load torque. Due to the presence of nonsinusoidal EFM and slot harmonics below 0.08 of nominal rotor speed (Figs. 9 and 10) in the IPMSM, oscillations of state variables occur. The sensorless control system is stable; however, the quality of rotor speed estimation and control is poor. Under small load torque command ($\sim$0.1–0.2 p.u.), amplitude of the stator current value increases. This inconvenience can be minimized by using the filtering method applied in a saliency-based solution, presented in [28] and [29]; or the extended control system structure [30]. However, the sensorless control system becomes complicated and computationally intensive in DSP. Additional analysis of

compensation methods should be carried out in the future and is not the subject of this article.

The main contribution of this article is the adaptive speed and position observer structure in which additional stabilization law was introduced. This allows for stable machine operation under nominal load torque value for motoring and regenerating machine modes; and for rotor speed of about 30–35 rpm and standstill [shown in Figs. 7(b) and 11(b) under the disturbances described earlier]. The idea is based on the introduction of additional law to the adaptive mechanism; which results from space vector theory. Additional stabilizing functions added to the speed adaptation mechanism (32) and to the position integrator (9) prevent: unstable working points; loss of synchronization in the IPMSM; and machine sticking. The transient of the stabilizing function (30) is not constant during machine's standstill operation [Figs. 7(b) and 11(b)]; thus, the introducing of permanent excitation in the observer structure ($u_{s\alpha,\beta} \neq 0$ for $\omega_r = 0$ [27]). The observers presented in, for example, [2], [3], [4], [5], and [28] are not stable for the low-speed range (below 0.15 p.u.) in the IPMSM with the nonsinusoidal EMF (this was implemented and checked in the laboratory stand). In the proposed solution, the observer system is based on the mathematical model of IPMSM in α-β reference frame and stabilized by using the mutual position of the vectors. This stabilization is effected by using the scalar product; which is introduced to the rotor position and rotor speed estimation laws in (30) and (33). Such an approach eliminates the potential errors in the estimated position and rotor speed, which are introduced to the observer structure based on the model in (d-q). The waveforms for the proposed observer structure can be compared with the HF method in [26]; to observer structure based on back-EMF [8]; and the speed and position encoder-based measurements. The waveform of the estimated rotor speed ($\hat{\omega}_{rEMF}$) based on the classical back-EMF observer [8] was shown in Fig. 10 for speed higher than the nominal speed and for standstill of the rotor, Fig. 11. Close to zero speed, the estimated speed and position have the undamped oscillations, and the estimated rotor speed error is above 0.06 p.u. for small speed range; and 0.08 p.u. for above nominal rotor speed [2.0 p.u., this is visible in Fig. 10(a)]. In order to compare the proposed sensorless structure with the encoder-based structure, the chosen waveforms are presented in Fig. 17. For this case, the waveforms are similarly to Fig. 9. The rotor speed has smaller level of oscillation (Fig. 17); however, the stator currents i_{sd}, i_{sq} contain measurement noises. The machine dynamic is similar. For speed close to zero, the saliency-based method (HF or LF injection) should be applied to avoid loss of synchronization in the IPMSM. This problem is averted by deploying the proposed sensorless control structure with the additional stabilizing functions. This indirectly injects higher harmonics and prevents the described phenomena.

In Table II, the comparison between three estimation schemes of rotor and position is presented. The first is proposed observer structure which is based on the rotor flux vector, the second is the classical EMF structure in the (dq) presented in [8] and [31], and the third is the structure with HF injection for position estimation [20], [31].
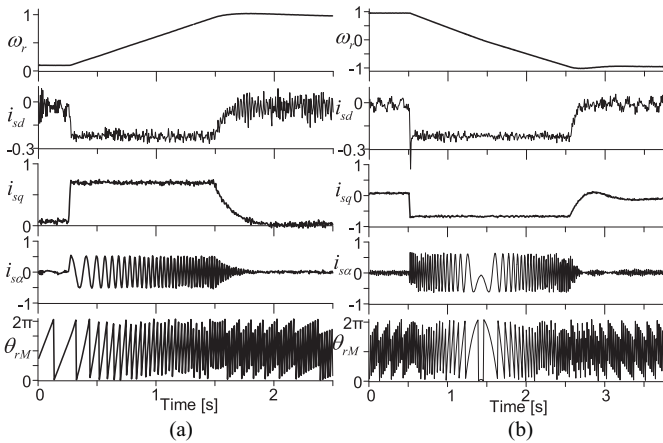
Fig. 17. IPMSM is (a) starting up to nominal speed, (b) reversing to nominal speed. The rotor speed, position, and stator currents are measured.

Fig. 18. Photograph of the experimental stand with the IPMSM clutched to dc machine.

TABLE II
COMPARISON OF SELECTED PROPERTIES OF THREE STRUCTURES OF THE OBSERVER (PROPOSED ROTOR FLUX OBSERVER, EMF, OBSERVER WITH HF)

Name	Proposed rotor flux observer	EMF-based structure [8]	Observer with HF injection [20, 31]
Machine startup/reverse	Stable	Stable	Stable
Avg. value of max. speed estimation error: - Low speed - high speed - Standstill	0.041 p.u. 0.025 p.u. 0.023 p.u.	0.052 p.u. 0.07 p.u. Unstable	0.038 p.u. 0.045 p.u. 0.022 p.u.
Stable work during uncertainties of parameters	Stable	Stable	Stable
Regenerating mode – avg. speed error	Stable 0.052 p.u.	0.07 p.u. or unstable for the load torque close to nominal	Stable 0.045 p.u.
Motoring operation mode	Stable	Stable	Stable

VI. CONCLUSION

This article presents the speed observer structure which is based on the mathematical model of the IPMSM machine for the stator current vector in the α-β reference frame. The rotor flux vector is estimated by using algebraic equations. The rotor speed is estimated by using the updated adaptive mechanism in which additional feedback is introduced to minimize estimation errors and to guarantee the robustness of the system. The rotor position is estimated from the integration of the estimated rotor speed value. The additional feedback was introduced to satisfy the observer's asymptotical stability. Proposed stabilization functions improve the stability of the observer structure without the HF injection of stator voltage [28] or stator current [29]. HF components are not directly injected by using the stator voltages but by using the proposed stabilization functions in the observer structure. Presented experimental tests for low rotor speed under regenerating mode, and standstill rotor operation confirm that the
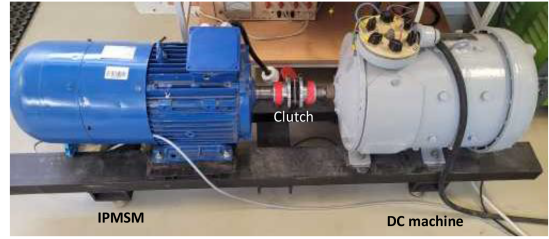
proposed sensorless control system is stable. Both the simulation and experimental results confirm that the observer structure is stable even if the parameters of IPMSM are different from its nominal values. The observer structure presented in this article was tested: for ultralow speed conditions with motoring and regenerating modes; with 150% of the load torque; and for speed higher than the nominal speed. Achieved results confirm that the proposed solution can be implemented in industrial applications.

APPENDIX

The parameters used in the mathematical model are defined

$$L_0 = 0.5(L_d + L_q), \ L_1 = L_d^{-1}\cos^2\theta_r + L_q^{-1}\sin^2\theta_r \quad (36)$$

$$L_2 = 0.5(L_d - L_q), \ L_3 = 0.5\left(\frac{1}{L_d} - \frac{1}{L_q}\right)\sin(2\theta_r) \quad (37)$$

$$L_4 = L_d^{-1}\sin^2\theta_r + L_q^{-1}\cos^2\theta_r \quad (38)$$

$$i_{\alpha 2} = i_{s\alpha}\cos 2\theta_r + i_{s\beta}\sin 2\theta_r \quad (39)$$

$$i_{\beta 2} = -i_{s\alpha}\sin 2\theta_r + i_{s\beta}\cos 2\theta_r. \quad (40)$$

The IPMSM machine nominal parameters are presented in Table I. The rotor iron to be made of electric steel sheets having nonlinear B-H characteristic.

The remanent flux density of PM is taken 1.15 T based on the Nd-Fe-B magnet property. The IPMSM has p = 2 poles, 50 Hz, number of slots is 36. The waveform of back-EMF has visible slot's harmonic shown in Fig. 8.

The photograph of the experimental stand is presented in Fig. 18. The IPMSM is coupled to the dc machine.

REFERENCES

[1] Y. Zhang, Z. Yin, C. Bai, G. Wang, and J. Liu, "A rotor position and speed estimation method using an improved linear extended state observer for IPMSM sensorless drives," *IEEE Trans. Power Electron.*, vol. 36, no. 12, pp. 14062–14073, Dec. 2021.

[2] C. J. Volpato Filho and R. P. Vieira, "Adaptive full-order observer analysis and design for sensorless interior permanent magnet synchronous motors drives," *IEEE Trans. Ind. Electron.*, vol. 68, no. 8, pp. 6527–6536, Aug. 2021.

[3] I. Boldea, M. C. Paicu, and G.-D. Andreescu, "Active flux concept for motion-sensorless unified AC drives," *IEEE Trans. Power Electron.*, vol. 23, no. 5, pp. 2612–2618, Sep. 2008.

[4] Z. Chen, M. Tomita, S. Doki, and S. Okuma, "An extended electromotive force model for sensorless control of interior permanent-magnet synchronous motors," *IEEE Trans. Ind. Electron.*, vol. 50, no. 2, pp. 288–295, Apr. 2003.

[5] M. Moradian, J. Soltani, A. Najjar-Khodabakhsh, and G. R. A. Markadeh, "Adaptive torque and flux control of sensorless IPMSM drive in the stator flux field oriented reference frame," *IEEE Trans. Ind. Inform.*, vol. 15, no. 1, pp. 205–212, Jan. 2019.

[6] Y. Zhao, W. Qiao, and L. Wu, "Improved rotor position and speed estimators for sensorless control of interior permanent-magnet synchronous machines," *IEEE J. Emerg. Sel. Topics Power Electron.*, vol. 2, no. 3, pp. 627–639, Sep. 2014.

[7] Y. Zhao, W. Qiao, and L. Wu, "An adaptive quasi-sliding-mode rotor position observer-based sensorless control for interior permanent magnet synchronous machines," *IEEE Trans. Power Electron.*, vol. 28, no. 12, pp. 5618–5629, Dec. 2013, doi: 10.1109/tpel.2013.2246871.

[8] A. Piippo, M. Hinkkanen, and J. Luomi, "Analysis of an adaptive observer for sensorless control of interior permanent magnet synchronous motors," *IEEE Trans. Ind. Electron.*, vol. 55, no. 2, pp. 570–576, Feb. 2008.

[9] L. Yuan, F. Xiao, J. Shen, M. Chen, Q. Shi, and L. Quan-feng, "Sensorless control of high-power interior permanent-magnet synchronous motor drives at very low speed," *IET Elect. Power App.*, vol. 7, no. 3, pp. 199–206, 2013.

[10] O. C. Kivanc and S. B. Ozturk, "Sensorless PMSM drive based on stator feedforward voltage estimation improved with MRAS multiparameter estimation," *IEEE/ASME Trans. Mechatron.*, vol. 23, no. 3, pp. 1326–1337, Jun. 2018.

[11] L. Sheng, W. Li, Y. Wang, M. Fan, and X. Yang, "Sensorless control of a shearer short-range cutting interior permanent magnet synchronous motor based on a new sliding mode observer," *IEEE Access*, vol. 5, pp. 18439–18450, 2017.

[12] Z. Li, S. Zhou, Y. Xiao, and L. Wang, "Sensorless vector control of permanent magnet synchronous linear motor based on self-adaptive super-twisting sliding mode controller," *IEEE Access*, vol. 7, pp. 44998–45011, 2019.

[13] G. Zhang, G. Wang, D. Xu, and N. Zhao, "ADALINE-network-based PLL for position sensorless interior permanent magnet synchronous motor drives," *IEEE Trans. Power Electron.*, vol. 31, no. 2, pp. 1450–1460, Feb. 2016.

[14] J. Han, "From PID to active disturbance rejection control," *IEEE Trans. Ind. Electron.*, vol. 56, no. 3, pp. 900–906, Mar. 2009.

[15] J. Li, Y. Xia, X. Qi, and Z. Gao, "On the necessity, scheme, and basis of the linear–nonlinear switching in active disturbance rejection control," *IEEE Trans. Ind. Electron.*, vol. 64, no. 2, pp. 1425–1435, Feb. 2017, doi: 10.1109/tie.2016.2611573.

[16] W. Xue, R. Madonski, K. Lakomy, Z. Gao, and Y. Huang, "Add-on module of active disturbance rejection for set-point tracking of motion control systems," *IEEE Trans. Ind. Appl.*, vol. 53, no. 4, pp. 4028–4040, Jul./Aug. 2017.

[17] Z. Gao, "On the centrality of disturbance rejection in automatic control," *ISA Trans.*, vol. 53, no. 4, pp. 850–857, 2014, doi: 10.1016/j.isatra.2013.09.012.

[18] R. Madonski and P. Herman, "Survey on methods of increasing the efficiency of extended state disturbance observers," *ISA Trans.*, vol. 56, pp. 18–27, 2015.

[19] G. Wang, H. Zhan, G. Zhang, X. Gui, and D. Xu, "Adaptive compensation method of position estimation harmonic error for EMF-based observer in sensorless IPMSM drives," *IEEE Trans. Power Electron.*, vol. 29, no. 6, pp. 3055–3064, Jun. 2014.

[20] G. Wang, T. Li, G. Zhang, X. Gui, and D. Xu, "Position estimation error reduction using recursive-least-square adaptive filter for model-based sensorless interior permanent-magnet synchronous motor drives," *IEEE Trans. Ind. Electron.*, vol. 61, no. 9, pp. 5115–5125, Sep. 2014.

[21] Y. Kano and N. Matsui, "Sensorless control of interior permanent magnet synchronous motor: An overview and design study," in *Proc. IEEE Workshop Elect. Mach. Des., Control, Diagnosis*, 2017, pp. 199–207.

[22] S. Bolognani, L. Tubiana, and M. Zigliotto, "Sensorless control of PM synchronous motors with non-sinusoidal back EMF for home appliance," in *Proc. IEEE Int. Elect. Mach. Drives Conf.*, 2003, vol. 3, pp. 1882–1888.

[23] G. Wang, Z. Li, G. Zhang, Y. Yu, and D. Xu, "Quadrature PLL-based high-order sliding-mode observer for IPMSM sensorless control with online MTPA control strategy," *IEEE Trans. Energy Convers.*, vol. 28, no. 1, pp. 214–224, Mar. 2013.

[24] M. X. Bui, D. Guan, D. Xiao, and M. F. Rahman, "A modified sensorless control scheme for interior permanent magnet synchronous motor over zero to rated speed range using current derivative measurements," *IEEE Trans. Ind. Electron.*, vol. 66, no. 1, pp. 102–113, Jan. 2019.

[25] G. H. B. Foo and M. F. Rahman, "Direct torque control of an IPM-synchronous motor drive at very low speed using a sliding-mode stator flux observer," *IEEE Trans. Power Electron.*, vol. 25, no. 4, pp. 933–942, Apr. 2010.

[26] S.-Y. Kim and I.-J. Ha, "A new observer design method for HF signal injection sensorless control of IPMSMs," *IEEE Trans. Ind. Electron.*, vol. 55, no. 6, pp. 2525–2529, Jun. 2008.

[27] A. Glumineau and J. L. Morales, *Sensorless AC Electric Motor Control Robust Advanced Design Techniques and Applications*. Berlin, Germany: Springer-Verlag, 2015.

[28] L. Gou, C. Wang, X. You, M. Zhou, and S. Dong, "IPMSM sensorless control for zero- and low-speed regions under low switching frequency condition based on fundamental model," *IEEE Trans. Transp. Electrif.*, vol. 8, no. 1, pp. 1182–1193, Mar. 2022.

[29] S.-I. Kim, J.-H. Im, E.-Y. Song, and R.-Y. Kim, "A new rotor position estimation method of IPMSM using all-pass filter on high-frequency rotating voltage signal injection," *IEEE Trans. Ind. Electron.*, vol. 63, no. 10, pp. 6499–6509, Oct. 2016.

[30] J.-S. Kim, S. Doki, and M. Ishida, "Improvement of sensorless control performance for IPMSM by suppression of harmonic current with Fourier transform and repetitive control," *IEEJ Trans. Ind. Appl.*, vol. 123, no. 4, pp. 1176–1184, 2007, doi: 10.1541/ieejias.123.1176.

[31] W. Goalin, Z. Guoqiang, and X. Dianguo, *Position Sensorless Control Techniques for Permanent Magnet Synchronous Machine Drives*. Berlin, Germany: Springer-Verlag, 2020.

Marcin Morawiec (Senior Member, IEEE) received the Ph.D. and D.Sc. degrees in electrical engineering from Gdansk University of Technology, Gdansk, Poland, in 2007 and 2017, respectively.

Since 2017, he has been an Associate Professor with Gdansk University of Technology. His main scientific activities are concentrated on multiscalar models, nonlinear control of any electrical machines, sensorless control, nonlinear control, backstepping control, adaptive observer backstepping, and sliding mode control.

Arkadiusz Lewicki (Senior Member, IEEE) received the Ph.D. and D.Sc. degrees in electrical drives from the Faculty of Electrical Engineering, Gdansk University of Technology, Gdansk, Poland, in 2003 and 2013, respectively.

He is currently with the Institute of Automatic Control of Electric Drives. His activities are concentrated on multilevel converters, pulsewidth modulation techniques, and nonlinear control systems.

Ikechukwu Charles Odeh (Senior Member, IEEE) received the B.Eng., M.Eng., and Ph.D. degrees in electrical engineering from the Department of Electrical Engineering, University of Nigeria, Nsukka, Nigeria, in 2002, 2006, and 2010, respectively.

His scientific activities are concentrated modulation techniques.